PERIDYNAMIC SIMULATION OF THERMAL RESPONSE OF HMX-BASED ALUMINIZED EXPLOSIVE

Yuxuan QI, Chunlan JIANG, Yubiao WEI, Wenyu XU, Zirui JIANG, Liang MAO*

State Key Laboratory of Explosion Science and Safety Protection, Beijing Institute of Technology, Beijing 100081, China

* Corresponding author; E-mail: mliang2015@bit.edu.cn

Peridynamic method has performed brilliant application prospects in many fields, especially the crack propagation and thermal-mechanical coupling problems. In this paper, a thermal peridynamic (TPD) simulation with McGuire-Tarver reaction kinetics model in the heat source is conducted for revealing the thermal response of energetic materials. This model takes account of multi-steps chemical reaction during the heating process and is appropriate for the crack condition. Herein, cook-off test simulation of octahydro-1,3,5,7-tetranitro-1,3,5,7-tetrazocine(HMX)-based aluminized explosive is carried out. Simulation results exhibit satisfactory accuracy compared with the previous experiments. The influence of heating rates and explosive component ratios on thermal response are also employed. The results show that heating rate plays an important rule on ignition time and position. The additions of HMX and AP are likely to trigger more violent exothermic chemical reaction during the ignition process. Particularly, cook-off model of warhead with crack is built and calculated. The results indicate that crack may lead to thermal accumulation and reaction aggravation of the explosive.

Keywords: *peridynamic; thermal response; reaction kinetics; energetic materials; crack condition*

1. Introduction

Extreme stimuli, such as heating [1-3] and impacting [4,5], have become great challenges for ammunition applications in modern battlefield, even causing serious casualties. Especially, violent combustion and detonation behaviors of the explosive in ammunition during fire hazards are likely to result in the wreck of military vessel. Therefore, reactivity and insensitivity of the energetic materials under various circumstances have attracted worldwide attention extensively. Many researches including experimental technique [6,7], numerical simulation [8-10] and mechanism investigation [11,12] were reported in previous years. Among them, cook-off tests equipped with temperature [13] and pressure [14] measurement systems were applied to explore the thermal response of explosive and ammunition effectively, conductive to the analysis of thermal decomposition, reaction evolution and product convection. The previous study [14] demonstrated that warhead structure influences the ignition behavior and reaction intensity significantly. Besides, cracks and voids in the charge would also contribute to the heat accumulation and reaction evolution [5]. Duan et al. [15] established combustion crack-network (CCN) model by theoretical analysis for safety design of the ammunition.

Liu et al. [16] adopted digital image correlation (DIC) technique in Brazilian disk test, and provided full-field deformation information of the crack propagation of PBX 9501. Although experimental and theoretical researches have been reported generally, simulation of explosive with cracks were still limited due to the singularity. For the finite element method, both modeling and computation are complicated if cracks exist, involving anomalous and bifurcate boundary treatment.

In the past decades, peridynamic approach proposed by Silling [17] has been developed for solving a series of scientific and engineering problems in many fields, such as composite materials [18], marine engineering [19] and aerospace industry [20]. This method handles governing equation using integral form instead of differential form, leading to distinctive advantages on the computation of discontinuity, especially the boundary positions and crack tips. Recently, peridynamic was extended to deal with ballistics and explosion problems gradually, which presented satisfactory calculation results. Kazemi [21] studied plastic deformation of the steel target under high-velocity impact using ordinary state-based peridynamic (OSB-PD) theory developed by Madenci and Oterkus [22]. Huang et al. [23] embedded a novel hybrid polymer-water model into non-ordinary state-based peridynamic (NOSB-PD), and realized the simulation of large deformation when soft material was penetrated by projectile. Zhu et al. [24] and Yang et al. [25] carried out peridynamic simulation on rock and concrete under explosion loading, and revealed their fracture characteristics in details. Besides, the allowance of natural evolution of cracks and voids improved its applications in the assessment of polymer bonded explosive (PBX). Deng et al. [26] built bond-based peridynamic (BB-PD) model of PBX consisting of explosive crystal and binder. It is found that inter-granular and trans-granular fracture behaviors can be captured in this simulation. Huang et al. [27] employed BB-PD model to investigate the dynamic damage behaviors of PBX confined in spherical steel shells. The effects of impact speed and elastic modulus on damage evolution of PBX was examined and discussed. Although peridynamic governing equation has been derived to solve the heat conduction issues [28], even the thermal-mechanical coupling problems [29]. Thermal response and energy release of energetic materials are lack of investigation by using peridynamic. However, chemical reactions and exothermic phenomena were rarely in consideration in previous work.

Here, we conducted a thermal peridynamic (TPD) simulation with McGuire-Tarver reaction kinetics model in the heat source, and built the TPD model of octahydro-1,3,5,7-tetranitro-1,3,5,7-tetrazocine(HMX)-based aluminized explosive cook-off test accounting for the influences of explosive components. The validity of this method was proved by comparing with existing research. Thermal response of the explosive under various conditions have been investigated and discussed in details. Furthermore, the cook-off process of warhead with crack in the charge were simulated and analyzed. This research conducted a TPD simulation for the thermal response of energetic materials and paves the way for its engineering applications.

2. TPD simulation for energetic materials

2.1. TPD formulation

Thermal response of the energetic materials under heating loading is mainly governed by the diffusion equation before the combustion and detonation. By substituting the spacial integral form into conventional equation, the diffusion equation in peridynamic framework [28] was built as follows:

$$\rho C_V \dot{\theta}(x,t) = \int_H f_h(\theta', \theta, x', x, t) dV_{x'} + h_s(x,t) \tag{1}$$

where ρ, C_v and θ are the density, specific heat capacity and temperature of the calculated point, respectively. h_s is the heat source of the calculated point, which can be obtained by the reaction kinetics model subsequently. In peridynamic framework, discrete points are influenced by the points in neighbourhood non-locally, which is called the horizon. x represents the coordinate of point that calculated at present, and x' represents the coordinate of point in its horizon, $V_{x'}$ represents its volume after modification. The associations between present point and its points in horizon are denoted by thermal bond pairwise function f_h in the integration.

The pairwise function f_h is associated with the micro-thermal potential z and temperature difference τ:

$$f_h = \frac{\partial z}{\partial \tau} \tag{2}$$

$$\tau = \theta'(x') - \theta(x) \tag{3}$$

The micro-thermal potential z can be written as follows:

$$z = \kappa \frac{\tau^2}{2|\xi|} \tag{4}$$

$$\xi = x' - x \tag{5}$$

where κ refers to the micro-thermal conductivity in peridynamic framework, and ξ refers to the relative position between calculated point and the point in its horizon.

By using the integration of micro-thermal potential and comparing it with the conventional theory, the relationship between micro-thermal conductivity and conventional thermal conductivity is built, as follows:

$$\kappa = \frac{6\lambda}{\pi \delta^4} \tag{6}$$

where λ refers to the conventional thermal conductivity, and δ refers to the radius of horizon.

In the numerical simulation, forward Euler method is used to process time iteration. Here, we obtain the discrete form of thermal peridynamic equation:

$$\theta^{n+1}(x,t) = \theta^n(x,t) + \frac{\sum_H f_h(\theta', \theta, x', x, t) \Delta V_{x'} + h_s(x,t)}{\rho C_V} \Delta t \tag{7}$$

where n and Δt represents the current time step and time interval, respectively.

2.2. Reaction heat source

During the heating process, chemical reactions of the components in the explosive are activated. Phase transition and thermal decomposition contribute to the variation of internal energy, performing endothermic or exothermic behaviors in the heat source. For most energetic components, this phenomenon is controlled by Arrhenius law. Here, we take the typical HMX-based aluminized

explosive as an example. This explosive mixture in this paper consists of HMX, Kel-F binder, Al and ammonium perchlorate (AP). Except the aluminum particles, the other components are all energetic. Reaction kinetics of HMX are simulated by McGuire-Tarver model, including four reversible kinetics steps [30]: (a) β-HMX ↔ δ-HMX, first order endothermic (b) β-HMX+δ-HMX ↔ δ-HMX, bimolecular endothermic (c) δ-HMX → products, first order endothermic (d) δ-HMX + products → products, bimolecular exothermic. The preceding steps are described by the following equations.

$$r_1 = \frac{k_p \theta}{h_p}\left[w_\beta \exp\left(\frac{\theta \Delta S_{1f} - E_{1f}}{R\theta} \right) - w_\delta \exp\left(\frac{\theta \Delta S_{1r} - E_{1r}}{R\theta} \right) \right] \tag{8}$$

$$r_2 = w_\beta w_\delta \frac{k_p \theta}{h_p}\left[\exp\left(\frac{\theta \Delta S_{2f} - E_{2f}}{R\theta} \right) - \exp\left(\frac{\theta \Delta S_{2r} - E_{2r}}{R\theta} \right) \right] \tag{9}$$

$$r_3 = w_\delta Z_3 \exp\left(-\frac{E_3}{R\theta} \right) \tag{10}$$

$$r_4 = w_\delta w_p Z_4 \exp\left(-\frac{E_4}{R\theta} \right) \tag{11}$$

where r with subscript 1 to 4 refer to the reaction rates in each step. w_β, w_δ and w_p represent the mass fractions of β-HMX, δ-HMX and products, respectively. k_p, h_p and R denote Boltzmann, Planck and ideal gas constants, respectively. ΔS_{1f} and ΔS_{2f} are the activation entropy in positive process, ΔS_{1r} and ΔS_{2r} are the activation entropy in reverse process. E_{1f}, E_{2f}, E_3 and E_4 are the activation energy in positive process, E_{1r} and E_{2r} are the activation energy in reverse process. Z_3 and Z_4 refer to the pre-exponential factors.

The variation of HMX phases can be calculated by using Euler or Runge-Kutta approach, the ordinary differential equations are as follows:

$$\frac{dw_\beta}{dt} = -r_1 - r_2 \tag{12}$$

$$\frac{dw_\delta}{dt} = r_1 + r_2 - r_3 - r_4 \tag{13}$$

$$\frac{dw_p}{dt} = r_3 + r_4 \tag{14}$$

Kel-F binder performs thermal decomposition and endothermic phenomenon [31]. This process is described by Frank-Kamenetskii reaction kinetics model [32]:

$$r_5 = Z_5 \exp\left(-\frac{E_5}{R\theta} \right) \tag{15}$$

where r_5, Z_5 and E_5 are reaction rate, pre-exponential factor and activation energy of the Kel-F binder.

Phase transition of AP occurs at 240℃ approximately. It is reasonable for the cook-off simulation to neglect this process [33]. Here, thermal decomposition of AP is described by Eq.(16):

$$r_6 = Z_6 \exp\left(-\frac{E_6}{R\theta}\right)\alpha_{AP}^{n}\left(1-\alpha_{AP}\right)^{m} \tag{16}$$

where r_6, Z_6, E_6 and α_{AP} are reaction rate, pre-exponential factor, activation energy and reaction extent of the AP, n and m are the reaction parameters. Liu et al. [31] suggest that n=1 and m=1.38, α_{AP} =0 when temperature is lower than 150℃ and α_{AP} =10^{-4} when temperature is higher than 150℃.

Based on the above derivation, we obtain the reaction heat sources from the phase transitions and thermal decomposition of HMX, binder and AP:

$$S_{HMX} = \sum_{i=1}^{4} \rho_i Q_i r_i \tag{17}$$

$$S_{Binder} = \rho_{Binder} Q_5 r_5 \tag{18}$$

$$S_{AP} = \rho_{AP} Q_6 r_6 \tag{19}$$

where Q with subscript 1 to 6 refer to the energy release of the reactions, and ρ with subscript 1 to 4 represent the densities of reactants in the HMX reaction steps. The variation of density in the reaction is neglected, and these densities equal to the density of HMX reactant. Due to the inertness of aluminum during the heating process before ignition, the reaction heat source of aluminum is zero.

Density, heat source and the heat parameters of the material point are obtained by the mixture law, which are associated with the explosive components and their reaction status.

$$\frac{1}{\rho} = \frac{1}{\varphi_{HMX}\rho_{HMX}} + \frac{1}{\varphi_{Binder}\rho_{Binder}} + \frac{1}{\varphi_{AP}\rho_{AP}} + \frac{1}{\varphi_{Al}\rho_{Al}} \tag{20}$$

$$S = \varphi_{HMX} S_{HMX} + \varphi_{Binder} S_{Binder} + \varphi_{AP} S_{AP} + \varphi_{Al} S_{Al} \tag{21}$$

$$\lambda = \varphi_{HMX} \lambda_{HMX} + \varphi_{Binder} \lambda_{Binder} + \varphi_{AP} \lambda_{AP} + \varphi_{Al} \lambda_{Al} \tag{22}$$

$$C = \varphi_{HMX} C_{HMX} + \varphi_{Binder} C_{Binder} + \varphi_{AP} C_{AP} + \varphi_{Al} C_{Al} \tag{23}$$

where φ with the subscript of explosive component refers to its mass fractions, and the other letters with these subscripts are the corresponding variables or parameters of these components.

2.3. Boundary and interface

In the cook-off test, heating process of the boundary is determined by the temperature controller and heating furnace. To this end, two layers points of the outside surface of the shell are set the temperature values obtained by the heating rate and time. Parts in the simulation contain air, shell and explosive. Six kinds of thermal bonds including A-A, S-S, E-E, A-S, S-E, E-A exist in this system, as shown in Fig.1. Among them, A-A, S-S and E-E bonds are located in the single material, which are considered as usual. Whereas, A-S, S-E and E-A bonds pass across two different materials in the

computation. For the simplification of the problem, we assume that the thermal conductivity of these bonds can be obtained by the average amount [28] in Eq.(24), due to it took a long time to finish the heating process in the slow cook-off test.

$$\kappa_{ab} = \frac{L_a + L_b}{\frac{L_a}{\kappa_a} + \frac{L_b}{\kappa_b}} \tag{24}$$

where κ_{ab}, κ_a and κ_b refer to the micro-thermal conductivity of interface, material a and b bonds, respectively. L_a and L_b represent the distances from material points to the interface.

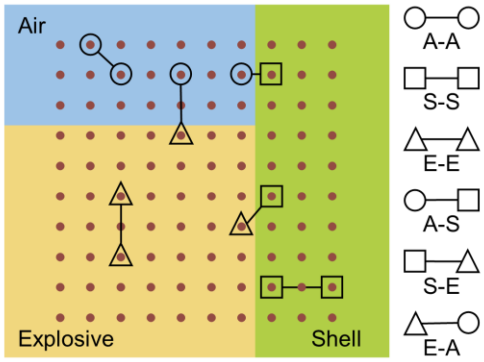

Fig. 1 Schematic diagram of bond categories in the simulation of cook-off test

2.4. Examples and parameters

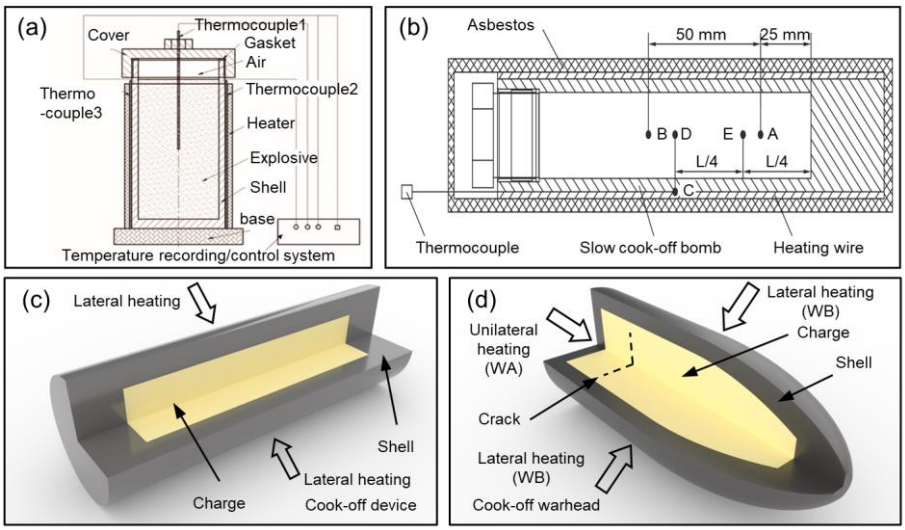

Fig. 2 Schematic diagram of cook-off devices and warhead: (a) and (b) Cook-off device reported by Liu et al. [31] and Dong et al. [34], (c) and (d) Cook-off device and warhead in this research

For the validity of TPD approach with reaction heat source, we replicate the experiments and simulations reported by Liu et al. [31] and Dong et al. [34]. The first experiment device mainly consists of GOLA-1 explosive (HMX:Al:AP:binder = 44:25:20:11, wt.%), thermocouple, air, heater, steel shell and cover. The length and diameter of this device are 106 mm and 58 mm, respectively. The length and diameter of the charge are 88 mm and 50 mm, respectively. The thickness of the shell is 4 mm, and there is 12 mm air gap between the charge and cover, as shown in Fig.2 (a). Heating rates are chosen as 1.0 and 1.5 K/min from the initial temperature of 298 K. The first simulations are meshed

into 84948 particles, including 43472 explosive particles, 35548 shell particles and 5928 air particles. The second experiment device was equipped with 4 mm steel shell and explosive with the mass ratios of HMX:Al:binder = 58:35:7. The length and diameter of the charge are 25 mm and 100 mm, respectively, as shown in Fig.2 (b). Heating rates are chosen as 0.5 and 1.0 K/min from the initial temperature of 393 K. The second simulation are meshed into 54984 particles, including 12100 explosive particles and 42884 shell particles.

Tab. 1 Numerical simulation conditions of the cook-off test with various component ratios

Number	HMX mass ratio (%)	Al mass ratio (%)	AP mass ratio (%)	Binder mass ratio (%)
A-1	50	30	10	10
A-2	50	20	20	10
A-3	50	10	30	10
B-1	60	10	20	10
B-2	50	20	20	10
B-3	40	30	20	10
C-1	60	20	10	10
C-2	50	20	20	10
C-3	40	20	30	10

Tab. 2 Numerical simulation conditions of the cook-off warhead

Number	Heating position	Crack existence
WA-N	Unilateral	No
WA-C	Unilateral	Yes
WB-N	Lateral	No
WB-C	Lateral	Yes

Furthermore, HMX-based aluminized explosive under different heating rates and with various component mass ratios are simulated and investigated. Fig.2 (c) depicts schematic diagram of cook-off device in our investigation. The diameters of charge and shell are 15 mm and 21 mm, and the length of charge and shell are 60 mm and 80 mm, respectively. Gauge point is set in the middle of charge. Explosive component mass ratios in the exploration of heating rates are HMX:Al:AP:binder = 50:20:20:10. Tab.1 shows the numerical simulation conditions of cook-off test with various component ratios at 1.0 K/min heating rate. Here, the research on Al:AP, HMX:Al and HMX:AP are represented by A, B and C, respectively. The cook-off device are meshed into 9680 particles, including 2580 explosive particles and 7100 shell particles. Finally, the cook-off simulations of warhead with and without adiabatic crack are employed. Although the cracks in the charge are distributed randomly and may perform various geometric features, a straight crack case is suitable and easily as a typical example. Here, we conduct an ogive warhead with 30 mm diameter and 4 mm thickness shell at 1.0 K/min, and the charge component ratios are HMX:Al:AP:binder = 50:20:20:10, as shown in Fig.2 (d). An adiabatic crack with the length of 16 mm in the diameter direction has been introduced 12 mm away from the bottom surface of the charge. Two different boundary conditions are employed in order to simulate the warhead in actual situations. As shown in Tab.2, WA refers to

warhead under unilateral heating and WB refers to warhead under lateral heating, while N and C represent without and with crack. The parameters of numerical simulation refer to the previous research [30-34]. The cook-off warhead are meshed into 12554 particles, including 4978 explosive particles and 7576 shell particles. In all the simulations of this investigation, the particle size is 1 mm, the horizon radius is 2.015 mm, and the time step is set as 0.01 s. The ignition time is recorded approximately when the reaction extents of HMX or AP arrive 50%.

3. Results and discussion

3.1. Validity of simulation

Computational and experimental results in the condition of Liu et al. [31] and Dong et al. [34] research are shown in Fig.3 (a), (b) and Fig.3 (c), (d), respectively. The comparison of TPD results and previous experiments demonstrates that the TPD method and parameters in this work are reliable and available. Fig.3 (a) indicates that thermal ignition occurs in the bottom annular region of the charge at 1.0 and 1.5 K/min. Temperature distribution at 1.0 K/min exhibits better homogeneous than 1.5 K/min, since the thermal energy from shell can diffuse more sufficiently in the charge. The lateral and bottom shell heat the charge collectively, leading to the heat accumulation and thermal ignition of the annular region. Temperature versus time curves show fine consistency between simulation and experiment, as shown in Fig.3 (b). The results show that temperature platforms emerge in the curves at 443 K approximately. This phenomenon can be interpreted as the phase transition of the explosive from β-HMX to δ-HMX, which have been observed in the simulation of Liu et al. as well. There are slight deviations between computational and experimental curves after the phase transition, due to the slight variation of density and specific heat capacity. However, ignition times at 1.0 and 1.5 K are 12180 and 8230 s in the TPD simulation, while ignition times are 11946 and 8070 s in the test. The relative errors

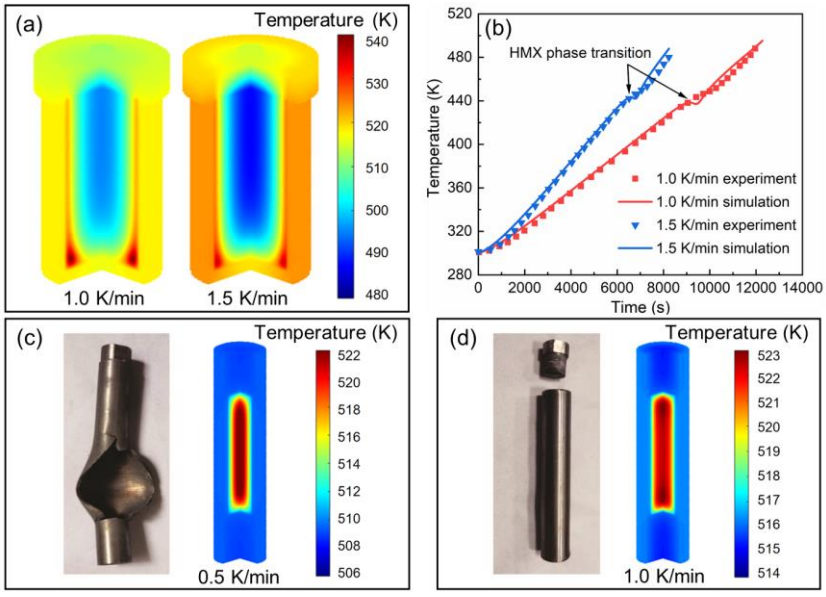

Fig. 3 Comparison of TPD results and previous experiments: (a) and (b) Computational and experimental results (tested by Liu et al.), (c) and (d) Computational and experimental results (tested by Dong et al.)

are less than 2.0%, indicating the satisfactory predictability of the method. For the large aspect ratio cook-off test, Dong et al. found that thermal ignition phenomena occur in the middle of tube at 0.5 K/min and in the end of tube at 1.0 K/min. Highly similar results are obtained by TPD method, high temperature region emerges in the middle of charge at 0.5 K/min and in the end of charge at 1.0 K/min, demonstrated that TPD method can capture the movement of ignition position.

3.2. Thermal response at different heating rates

Fig.4 shows simulation results of the cook-off device at different heating rates. Temperature distribution contours indicate that ignition position has a tendency to move from the central portion to the ends of the charge with the increase of heating rates, as shown in Fig.4 (a). When the heating rate reaches 2.0 K/min, high temperature region expands in the radial direction symmetrically, which tends to form an annular distribution. The reason for this phenomenon is that there is not enough time for the heating energy to diffuse into the central portion uniformly. Fig.4 (b) illustrates temperature versus time curves at different heating rates in the gauge point. With the decrease of heating rates, temperature curves become flatter and the ignition time delays, due to the slope of curves are mainly dominated by heating rates before violent exothermic chemical reaction occurs. The ignition times are approximately 24950, 12980, 8870 and 6770 s at the heating rates of 0.5, 1.0, 1.5 and 2.0 K/min, respectively. HMX phase transition platform become steeper with the increase of heating rates. The duration of phase transition increases from 220 s to 650 s with the decrease of heating rate from 2.0 K/min to 0.5 K/min approximately. One possible explanation is that rapid heating process promotes the phase transition speed at high heating rate. Fig.4 (c) depicts the typical mass fraction curves during

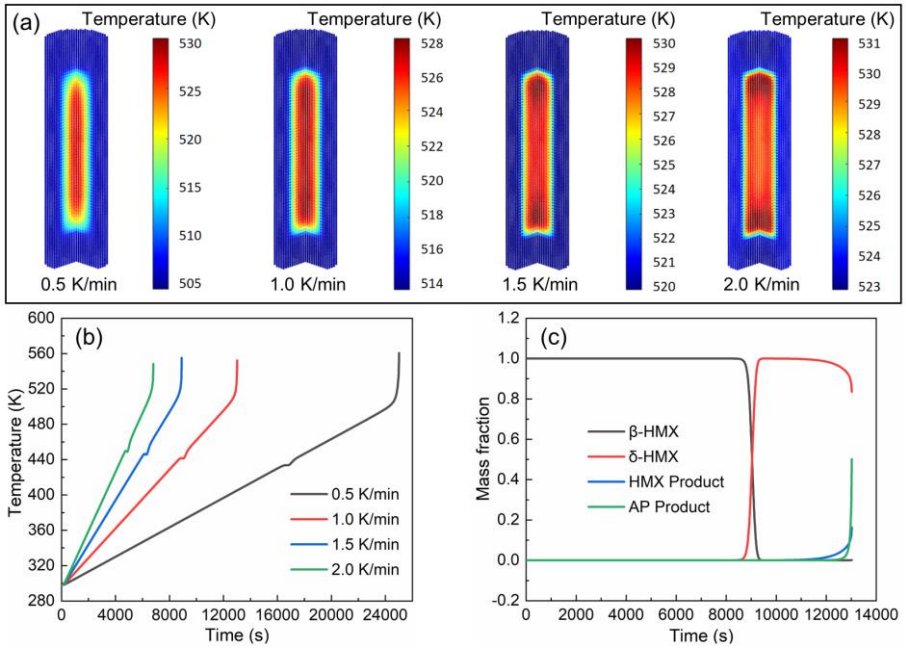

Fig. 4 Simulation results of the cook-off device at different heating rates: (a) Temperature distribution when ignition phenomena occur, (b) Temperature versus time curves, (c) Mass fractions of the explosive components at 1.0 K/min heating rate

the heating process at 1.0 K/min heating rate. Distinctly, β-HMX decreases while δ-HMX increases rapidly at the moment of 9060 s, corresponding to the HMX phase transition platform in temperature curves. At the end of heating process, δ-HMX and AP are stimulated to react simultaneously.

Therefore, the chemical reaction of HMX and AP should be employed when the ignition phenomenon is triggered. However, heating rates play an important rule on the ignition position and time of the cook-off device, corresponding to the experiment results of the previous research [14,34].

3.3. Thermal response with various component ratios

Based on the application demands, the component ratios of HMX-based aluminized explosive are usually adjustable in practice. On this occasion, thermal decomposition and ignition behavior of the charge are likely to change, even though equipped in the identical structure. Fig.5 (a) and (b) show the effect of Al:AP component ratio on the thermal response. In macroscopic scale during the whole heating process, few diversities can be observed generally, due to the entire temperature range is too large for investigation in details. However, there are obvious distinctions near the phase transition and ignition time. It is found that temperature rise delays with the increase of Al:AP ratio, resulting from the addition of Al increases the specific heat capacity of the explosive slightly. Interestingly, A-3 condition with rich AP exceeds the temperature curve in the condition of A-1 with poor AP. At the moment of 12950 s, A-3 condition has formed prominent high temperature region near the ends of charge. The effect of AP on the temperature rise near the end of cook-off process seems to overcome the influence of Al, due to its fast exothermic chemical reaction. Fig.5 (c) and (d) illustrate the effect of HMX:Al component ratio on the thermal response. With the increase of Al addition, temperature in the gauge point has the similar tendency with the condition of Al:AP, due to the high specific heat capacity of Al and the energy release of HMX. The difference is that the decrease of HMX smooths the temperature variation during the phase transition. Fig.5 (e) and (f) depict the effect of HMX:AP component ratio on the thermal response. Under this circumstance, the influence of AP on temperature curves near the HMX phase transition is similar to Al. Meanwhile, simulation contours and curves demonstrate that temperature when the ignition occurs rise barely with the increase of AP, indicating that HMX:AP component ratio has little influence on the thermal response before the violent reaction emerges.

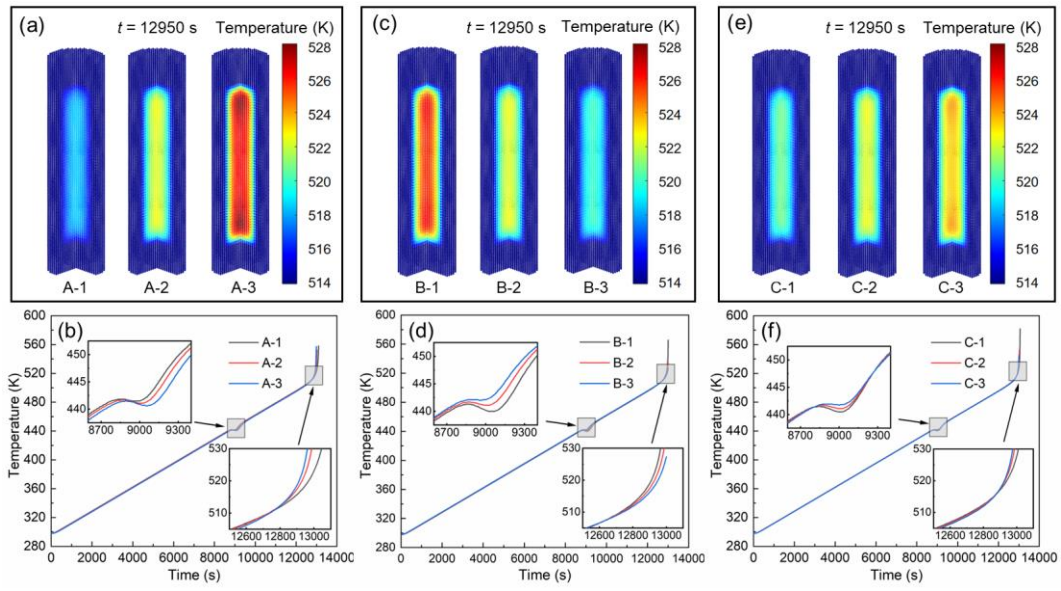

Fig. 5 Temperature results with various component ratios: (a) and (b) Various Al:AP ratios, (c) and (d) Various HMX:Al ratios, (e) and (f) Various HMX:AP ratios

As mentioned above, the addition of Al in the explosive cause faster temperature rise to some extent, while AP and HMX component are likely to promote the exothermic chemical reaction. Especially, high AP and HMX component additions may improve the violent combustion and detonation. Based on the thermal safety consideration, the deceleration of temperature rise during heating process in the rich Al explosive and the relaxation of chemical reaction before ignition time in the rich AP or HMX are necessary for the insensitive ammunition design.

3.4. Thermal response of the warhead with crack

Fig.6 presents the heating process and thermal response of the warhead under different conditions. For the warhead under unilateral heating, thermal energy transmits from the bottom to top gradually, resulting in a temperature gradient in the warhead. At the same axial position, the temperature rises more slowly in the charge than shell, due to the explosive have a lower specific heat capacity. Temperature distribution demonstrates that the ignition phenomenon occur in the bottom of charge at 13400 s approximately. However, the existent of crack has an effect on blocking heat conduction in the charge to some extent. This effect generates thermal accumulation under the crack, leading to the ignition position moves up as well as higher temperature distribution in this region. For the warhead under lateral heating, thermal energy transmits from the surrounding and bottom of the charge simultaneously. The explanation for this phenomenon is that the steel has an excellent thermal conductivity, leading to the temperature rises rapidly in the bottom of shell. Meanwhile, there is a low temperature region in the top of charge, due to the lack of heating around the ogive portion. In this case, ignition position occurs at 13050 s approximately and separates from the bottom of charge, while high temperature region becomes more homogeneous and larger. It is noted that the crack cut off the high temperature region and exacerbate the thermal acceleration under the crack, leading to higher temperature at the same time. Therefore, cracks are likely to enhance the thermal decomposition of the charge and trigger more violent combustion or deflagration reaction, even cause the undesirable detonation behavior.

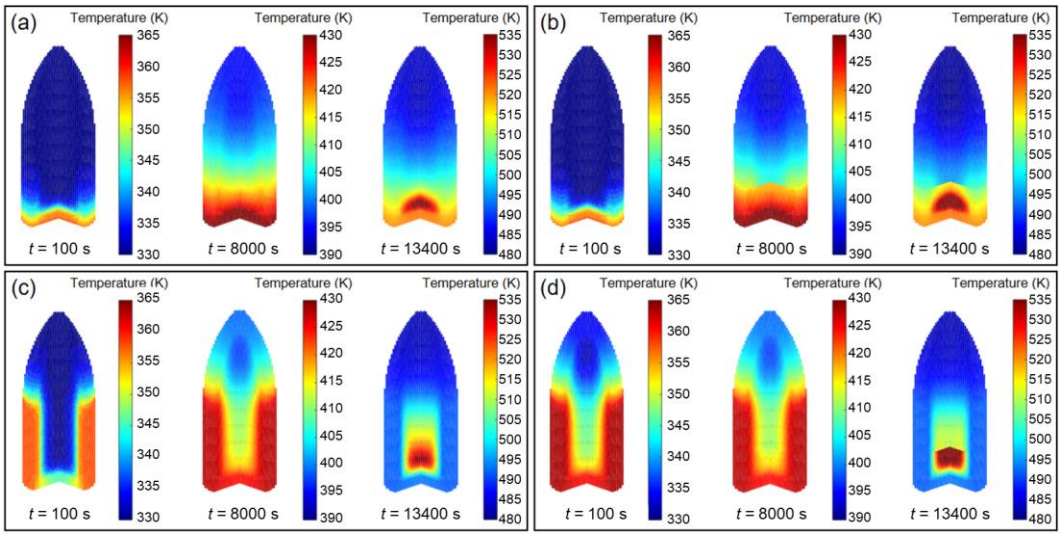

Fig. 6 Heating process and thermal response of the warhead: (a) WA-N, (b) WA-C, (c) WB-N, (d) WB-C

To further reveal the chemical reaction behavior of the charge, reaction extent contours and curves are extracted, as shown in Fig.7. Chemical reaction of HMX mainly occurs in the bottom of the charge under unilateral heating while it performs a gradient distribution under lateral heating, as shown in Fig.7 (a). Apparently, a high reaction extent point emerges above the bottom surface of the charge in WA-C condition, indicating that crack may move up the ignition position under this circumstance. By contrast, HMX product mass fraction of the same region merely increases fewer while high reaction extent point has not appeared in WB-C condition. Chemical reaction of AP concentrates near the interface between charge and shell achieves a high reaction level under unilateral heating while it presents an upward trumpet-like gradient distribution under lateral heating, as shown in Fig.7 (b). When the crack emerges in the charge, the AP product distribution under unilateral heating maintains its profile and expands upwards slightly, while the chemical reaction of AP performs enhancement in the annular region between crack and bottom under lateral heating.

As mentioned above, the bottom portion of charge has a significant tendency to accumulate the heating energy and grow into violent exothermic chemical reaction in both lateral and unilateral cases whether there is a crack or not. Fig.7 (c) and (d) show the reaction extents at the axis position from the bottom of shell in these cases. The chemical reactions of WA cases perform local enhanced characteristic while WB cases are more homogeneous. It is noted that HMX contributes to the thermal accumulation primarily, the existence of crack may lead the high reaction region moving upwards in the charge. For the thermal safety consideration, charge quality monitoring and sensitivity reduction measure are suggested to be taken into account in the bottom region of the ammunition.

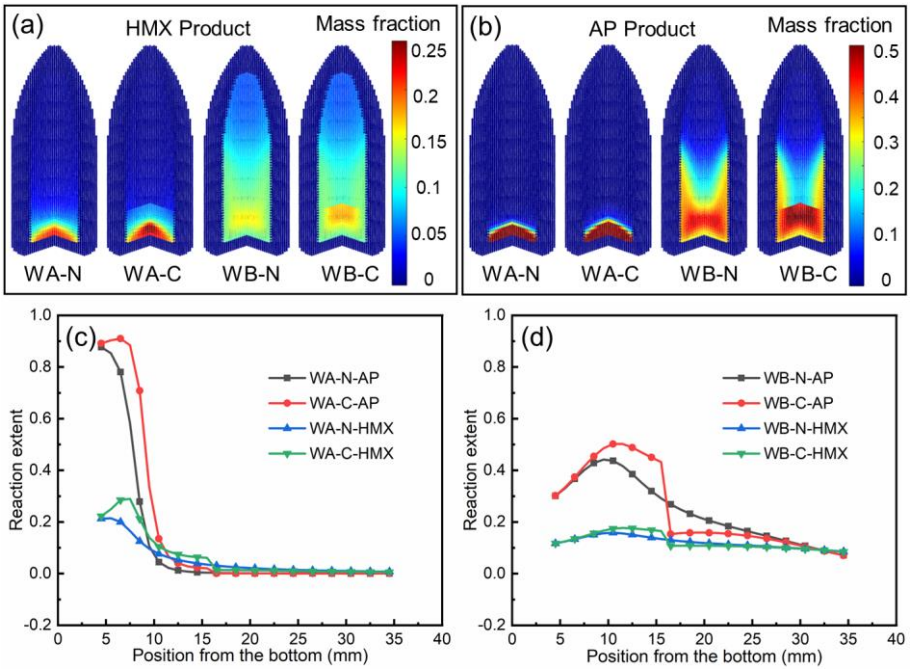

Fig. 7 Reaction extent of explosive components: (a) and (b) HMX and AP distribution, (c) and (d) Reaction extents at different positions of WA and WB

4. Conclusions

A thermal peridynamic (TPD) simulation with McGuire-Tarver reaction kinetics model was built for the thermal response issue of energetic materials as well as the problem with charge cracks.

The previous experimental results proved its validity, and more investigation on HMX-based aluminized explosive has been carried out. The main conclusions are drawn as follows:

- Thermal decomposition and ignition behavior could be simulated accurately by TPD approach with reaction heat source. Previous works demonstrated that the computational temperature curves correspond to the experimental results. The HMX phase transition platform and the rapid temperature rise during ignition have been observed obviously in the numerical simulation.
- Heating rate have an effect on ignition time and position. The additions of AP and HMX may trigger more violent chemical reaction, even though Al promote heat conduction before the ignition. The influence of HMX:AP on thermal response seem to be not distinctive. The variation of explosive components can be taken into account by using the computational code.
- The computational code was available to simulate the thermal response of warhead with crack in the charge. For the warheads which have the similar structure and size to the case in this research, the existence of crack may cause thermal accumulation in the bottom of charge, leading to more sufficient exothermic reaction of the explosive. Therefore, charge quality monitoring and sensitivity reduction measure are suggested to be taken into account for the thermal safety.

Conflict of interest

The authors declare no financial or commercial conflict of interest.

Acknowledgement

This research was funded by National Natural Science Foundation of China (No.12002045) and State Key Laboratory of Explosion Science and Safety Protection, Beijing Institute of Technology (QNKT22-09).

References

[1] Kou, Y. F., *et al.*, Assessing the thermal safety of solid propellant charges based on slow cook-off tests and numerical simulations, *Combustion and Flame, 228* (2021), pp. 154–162

[2] Wen, Q., *et al.*, Numerical analysis of response of a fuze to cook-off, *Journal of Energetic Materials, 37* (2019), 3, pp. 340–355

[3] Zhu, M., *et al.*, Numerical and experimental study on the response characteristics of warhead in the fast cook-off process, *Defence Technology, 17* (2020), 4, pp. 1444–1452

[4] Hanina, E., *et. al.*, Prediction of low-velocity-impact ignition threshold of energetic materials by shear-band mesoscale simulations, *Journal of Energetic Materials*, *36* (2018), 3, pp. 325–338

[5] Parker, G. R., *et al.*, Direct observation of frictional ignition in dropped HMX-based polymer-bonded explosives, *Combustion and Flame, 221* (2020), pp. 180–193

[6] Dickson, P. M., *et al.*, Thermal cook–off response of confined PBX 9501, *Proc. R. Soc. Lond. A, 460* (2004), 2052, pp. 3447–3455

[7] Hobbs, M. L., *et al.*, Vented and sealed cookoff of powdered and pressed ε-CL-20, *Journal of Energetic Materials, 39* (2020), 4, pp. 432–451

[8] Asante, D. O., *et al.*, CFD cook- off simulation and thermal decomposition of confined high energetic material, *Propellants, Explosives, Pyrotechnics, 40* (2015), 5, pp. 699–705

[9] Gross, M. L., *et al.*, Considerations for fast cook-off simulations, *Propellants, Explosives, Pyrotechnics, 41* (2016), 6, pp. 1036–1043

[10] Ye, Q., Yu, Y. G., Numerical simulation of cook-off characteristics for AP/HTPB, *Defence Technology, 14* (2018), 5, pp. 451–456

[11] Myint, P. C., Nichols, A. L., Thermodynamics of HMX polymorphs and HMX/RDX mixtures, *Ind. Eng. Chem. Res., 56* (2016), 1, pp. 387–403

[12] Gu, J. S., *et al.*, Kinetic modeling of liquid phase RDX thermal decomposition process and its application in the slow cook- off test prediction, *Propellants, Explosives, Pyrotechnics, 46* (2021), 6, pp. 935–943

[13] Sahin, H., *et al.*, Development of a design methodology against fast cook- off threat for insensitive munitions, *Propellants, Explosives, Pyrotechnics, 41* (2016), 3, pp. 580–587

[14] Wang, X. Y., *et al.*, Cook- off characteristics of NTO/HMX- based plastic- bonded explosives in a shaped charge, *Propellants, Explosives, Pyrotechnics, 48* (2023), 3, e202200206

[15] Duan, Z. P., *et al.*, Combustion crack-network reaction evolution model for highly-confined explosives, *Defence Technology, 26* (2023), pp. 54–67

[16] Liu, C., Thompson, D. G., Deformation and failure of a heterogeneous high explosive, *Philosophical Magazine Letters, 92* (2012), 8, pp. 352–361

[17] Silling, S. A., Askari, E., A meshfree method based on the peridynamic model of solid mechanics, *Computers & Structures, 83* (2005), 17, pp. 1526–1535

[18] Zhan, J. M. *et al.*, A rate-dependent peridynamic model for predicting the dynamic response of particle reinforced metal matrix composites, *Composite Structures, 263* (2021), pp. 113673

[19] Zhang, Y., *et al*., Peridynamic analysis of ice fragmentation under explosive loading on varied fracture toughness of ice with fully coupled thermomechanics, *Journal of Fluids and Structures, 112* (2022), 103594

[20] Wang, H., *et al.*, Peridynamics-based analysis on fracture behaviors of a turbine blade shroud, *Engineering Fracture Mechanics, 295* (2024), 109817

[21] Kazemi, S. R., Plastic deformation due to high-velocity impact using ordinary state-based peridynamic theory, *International Journal of Impact Engineering, 137* (2020), 103470

[22] Madenci, E., Oterkus, S., Ordinary state-based peridynamics for plastic deformation according to von Mises yield criteria with isotropic hardening, *Journal of the Mechanics and Physics of Solids, 86* (2016), pp. 192–219

[23] Huang, J. S., *et al.*, A hybrid polymer–water peridynamics model for ballistic penetration damage of soft materials, *Computer Methods in Applied Mechanics and Engineering, 415* (2023), 116216

[24] Zhu, F., Zhao, J. D., Peridynamic modelling of blasting induced rock fractures, *Journal of the Mechanics and Physics of Solids, 153* (2021), 104469

[25] Yang, S. Y., *et al.*, Explosion damage analysis of concrete structure with bond-associated non-ordinary state-based peridynamics, *Engineering with Computers*, *39* (2023), 1, pp. 607–624

[26] Deng, X. L., Wang, B., Peridynamic modeling of dynamic damage of polymer bonded explosive, *Computational Materials Science*, *173* (2020), 109405

[27] Huang, Y. F., *et al.*, Peridynamic investigation of dynamic damage behaviors of PBX confined in spherical steel shells, *Mechanics of Materials*, *172* (2022), 104389.

[28] Oterkus, E., Peridynamics for the solution of multiphysics problems, Ph. D. thesis, The University of Arizona, Arizona, US, 2015

[29] Oterkus, S., *et al.*, Fully coupled peridynamic thermomechanics, *Journal of the Mechanics and Physics of Solid*, *64* (2014), pp. 1–23

[30] Perry, W. L., *et al.*, Impact-induced friction ignition of an explosive: Infrared observations and modeling, *Journal of Applied Physics*, *108* (2010), 8, 084902

[31] Liu, Z.R., *et al.*, Cook-off test and numerical simulation of HMX-based cast explosive containing AP, *Chinese Journal of High Pressure Physics*, *36* (2022), 5, pp. 173–182

[32] Tarver, C. M., Koerner, J. G., Effects of Endothermic Binders on Times to Explosion of HMX- and TATB-Based Plastic Bonded Explosives, *Journal of Energetic Materials*, *26* (2008), 1, pp. 1–28

[33] Boldyrev, V. V., Thermal decomposition of ammonium perchlorate, *Thermochimica Acta*, *443* (2006), 1, pp. 1–36

[34] Dong, Z. L., *et al.*, Cook-off characteristics of HMX-based pressed charges with different sizes, *Chinese Journal of High Pressure Physics*, *38* (2024), 2, pp. 1–10

Received: 01.06.2024.
Revised: 18.07.2024.
Accepted: 29.07.2024.